CONCEPT AND ANALYSIS OF A SEMI-PASSIVE ARM AND ROV SYSTEM

Valmar Pereira Cabral Junior
Brazilian Navy Shipyard at Rio de Janeiro / Brazilian Navy
Production Department, 17° building, 3° floor
Ilha das Cobras - Centro - CEP 20091-000 Rio de Janeiro – RJ, Brazil
Tel.: 3849-6246 / 2253–6583
email: valmarpc@terra.com.br,

Vitor Ferreira Romano
Federal University of Rio de Janeiro E.E. / COPPE
Mechanical Engineering Department – Robotics Laboratory
Centro de Tecnologia, bloco G, sala 204
P. Box - 68503 - CEP 21945-970 Rio de Janeiro – RJ, Brazil
Tel.: 2562 – 8404 / 2562-7764
email: romano@serv.com.ufrj.br

Abstract: *The main purpose of this work is to present some of the technical fundamental principles to be used in the development of a Semi-Passive mechanical Arm (SPA), conceived to operate in deepwater oil exploration facilities, as a support to ROV (Remotely Operated Vehicles) during its interventions in sub sea scenarios. The kinematics and dynamic mathematical model of the semi-passive arm includes hydrodynamic forces and moments, due to buoyancy and the fluid drag caused by the interaction of the arm with the underwater environment. A three degree-of-freedom simplified model of the arm was constructed, so that its dynamical behavior could be investigated on site. Tests were performed for different arm configurations in ground conditions with a commercial data acquisition system based on infrared cameras, to obtain kinematics parameters of each link of the arm. These parameters were used as input data for the dynamical equations in order to find the nominal torque at the joints. A comparison is made between dynamic equations for the on ground and underwater conditions. The SPA concept is patent pending.*

Keywords: *underwater robotics, semi-passive arm, ROV, hydrodynamics modeling.*

1. Introduction

There are deepwater operations in oil exploration facilities that require precise position control of Remotely Operated underwater Vehicles (ROV) in a worksite limited to a few meters in the neighborhood of some underwater structure, where the ROV is performing its tasks. These are mainly drill and construction support, pipe survey and installation, underwater tool deployment and valve manipulation (Romano, 1997, Liu, 2000). The maintenance of the installed sub sea facilities involves periodic inspections of the equipments, and occasional interventions and repair that may include replacement of components. Today, most work and inspection activities are accomplished by Remotely Operated Vehicles (ROV's) instead of divers or manned underwater vehicles. Compared to manned submersible vehicles, ROV's can be used not only with less risk but also at greatly reduced cost (STN, 2001).

The ROV performance in conventional teleoperation control mode depends on the skill of its operator in controlling the vehicle and its payload in real time. This is more evident for complex tasks, where the operator must deal with instability problems due to unpredictable behavior of marine currents, time delay in data transmission for long distances between teleoperation centre and ROV worksite, and eventually low mobility related to high inertia ROV's. Computer aided teleoperation is been used to improve operator's decision capability, as an integrated environment of measurement system devices as inertial navigation, optical sensors (laser), hydroacustic sensors (sonar), taut-wire, vision systems. (Romano, 1997).

Activities related to manipulation of underwater equipment require the installation of a manipulator arm at the ROV, Fig. (1). In this case, any motion of the manipulator arm will induce reaction forces and moments that disturb the position and attitude of the supporting base vehicle, raising many problems to the control of ROV systems.

The same occurs if a ROV and manipulator arm system carries a payload, due to the addition of mass and inertia, resulting in a change of its center of gravity and consequently its equilibrium configuration. These phenomena happen due to the lack of a fixed base to transmit the force and moments originated by the interaction of the arm with the intervened environment, as occurs in industrial manipulators rigidly fixed at the ground (Cabral, 2002). Basically, there are two approaches to avoid this operational problem: the operator can use the ROV thrusters to compensate the perturbation or a grabber arm is installed at the ROV, so that a rigid link is established with the underwater facility to be intervened.

The underwater oilfield task will determine the type of ROV to be employed. Huge (massive) ROV's are necessarily used to perform tasks such as lifting heavy objects, while medium and small ROV's are used to inspection and manipulation of low-weight devices.

Precision tasks like positioning of the drill system always require huge ROV's to guarantee its stability. High inertia ROV's result in less positioning deviations caused by external perturbations, such as the marine current action and eventual force/torque originated from the interacting system.

Fig. 1. ROV with manipulator and grabber arms (Seaeye, 2003).

2. Semi-passive Arm Concept

The Semi-Passive mechanical Arm (SPA) is a new concept of structural support to ROV's, designed to increase their rigidity and precision during interventions in sub sea facilities.

The SPA is characterized by a rigid structure fixed at the sea bed and a mechanism formed by rigid links connected by revolute (rotational) or prismatic joints.

No actuators are installed at the joints, but brakes.

The combination of joints with activated brakes (locked) or not activated brakes (unlocked) permit the ROV to move in preferential directions, even if external perturbations like marine currents occur during the execution of a task. The ROV thrusters are still the unique source of mechanical power needed to move the ROV itself and the energy to activate brakes can be furnished by a dedicated conductor from umbilical cable, so that no energy is drained from ROV.

In figures (3) and (4) is present an example of SPA-ROV system in a gantry configuration with four degree-of-freedom (three prismatic and one revolute joints). In this case, the underwater facility to be intervened (Wet Christmas Tree - WCT) is located inside the SPA-ROV workspace.

In this example, three operational phases can be defined, as indicated in Fig. (3a) and Fig. (4): the approach phase (positions 1 to 2a), where the ROV is moving towards the SPA connector device; the connecting phase (position 2a), related to the ROV attachment with the SPA; and the intervention phase (position 3), concerning the SPA-ROV system workspace nearby the working zone.

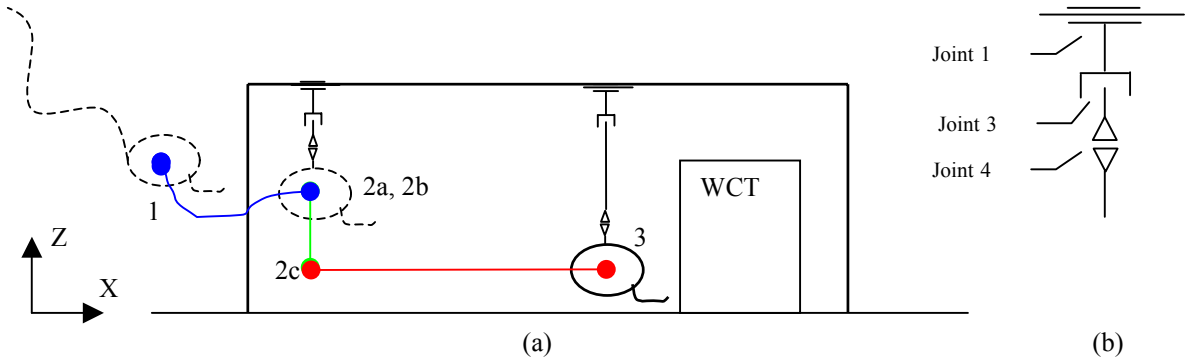

Figure 3. (a) Scheme of a SPA-ROV system scenario. (b) Schematic representation of joints 1, 3 and 4.

The trajectory of the SPA-ROV system from point 2a to point 3, can be described by a sequence of actuated (L – locked) and not actuated (U – unlocked) brakes, according to Table (1). Once the SPA-ROV system achieves the working zone, the brakes will be actuated or not according to the required intervention planning. When all brakes are in active configuration, the SPA-ROV system will behave as a fixed base manipulator, increasing its structural rigidity, payload capacity, precision and repeatability.

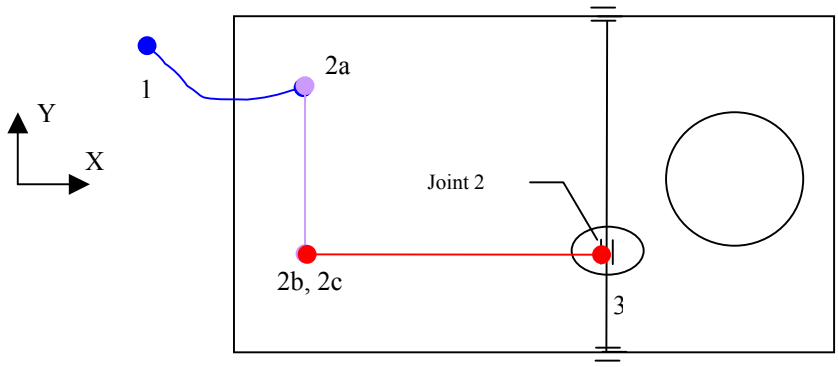

Figure 4. Description of the SPA-ROV system movements.

Table 1. Brake state conditions for the trajectory from point 2a to point 3.

MOTION From	To	Joint 1	Joint 2	Joint 3	Joint 4
2a	2b	L	U	L	L
2b	2c	L	L	U	L
2c	3	U	L	L	L

The system should be dimensioned so that ROV thrusters give the necessary power and the SPA brakes the motion constraints, to overcome the unpredictable hydrodynamic forces induced by marine currents.

A different configuration for the SPA-ROV system, such as the open kinematics chain presented in Figure (5), will operate in a similar mode as the gantry system. Despite its compact dimensions and weightless if compared to the previous system, its rigidity will decrease considerably. The choice of a SPA configuration is strictly dependent on the sub sea environmental conditions; the operational requirements and characteristics of the underwater facility to be intervened; and SPA performance indexes such as its dynamical behavior, maneuverability, achievable workspace, and so on. Actual technologies applied to ROV systems must be carefully considered (Andrews, 1993; Assayag, 1998; King, 1969), and also SPA mechanical design aspects (Rivin, 1998).

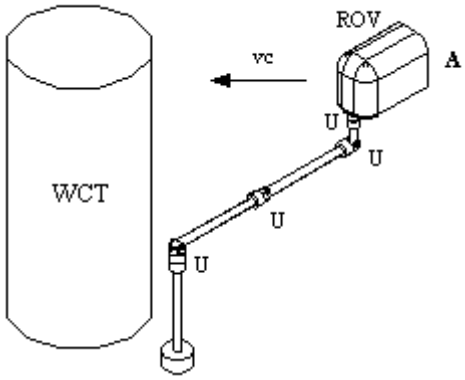

Figure 5. SPA-ROV system configured as open kinematics chain.

4. SPA Modeling

4.1. Model kinematics

The effects of drag and buoyancy forces due to fluid interaction on SPA-ROV system can disturb considerably its performance. Researches performed by Janocha (1991) and Lévesque (1994), with manipulators in a fluid environment, gave important indications about the best way to dispose the joints, the links and brakes in order to improve the SPA-ROV system performance.

The authors decided to investigate the fundamental principles concerning the equations involved in the interaction of SPA and fluid environment. The model adopted is configured as an open kinematics planar chain mechanism formed by one base, three revolute joints (J_1, J_2 and J_3) and three rigid links (L_1, L_2 and L_3), as indicated in Fig. (6a).

The tree joints can be locked or unlocked according to the combinations described in Table (2). In Figure (6b) and is illustrated the reference frames (RF) for each link and in Table (3) a summary of the Denavit and Hartenberg parameters of the model (Sciavicco, 1995).

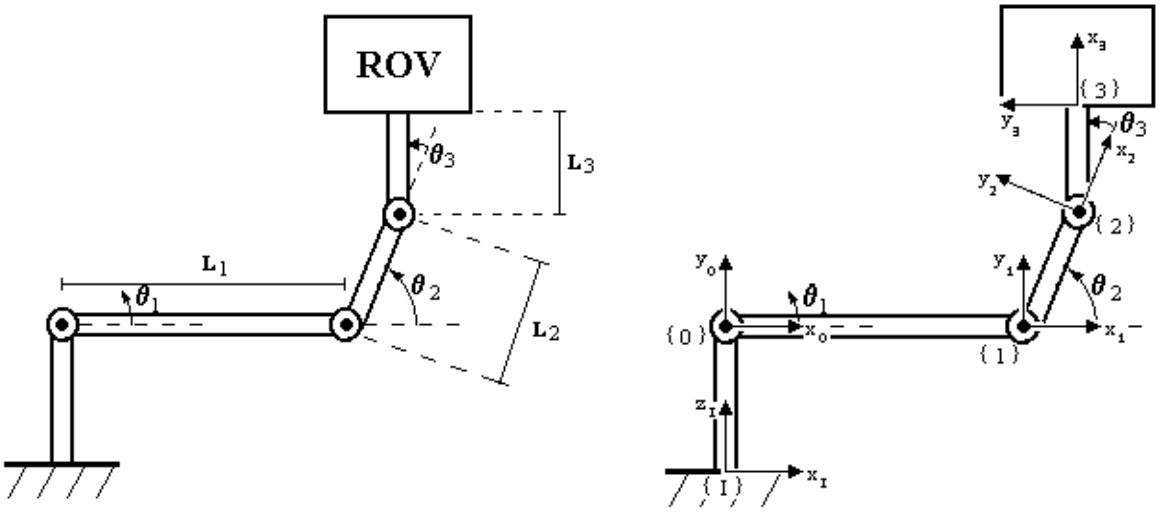

(a) (b)

Figure 6(a). Model investigated. (b). Inertial and local reference frames.

Table 2. Brakes logical combinations (L – locked, U – unlocked).

Combination	Joint 1	Joint 2	Joint 3
1	U	U	U
2	L	U	U
3	U	L	U
4	U	U	L
5	L	L	U
6	L	U	L
7	U	L	L

Table 3. Denavit-Hartenberg parameters.

Link i	a_i	α_i	d_i	θ_i
1	L_1	0	0	θ_1
2	L_2	0	0	θ_2
3	L_3	0	0	θ_3

The transformations matrices between adjacent frames will result in a matrix that represents the position and orientation of the arm's end-effector in relation to its base, as showed in Eq. (1).

$$ {}^{0}T_{3} = \begin{bmatrix} \cos(\theta_1+\theta_2+\theta_3) & -\text{sen}(\theta_1+\theta_2+\theta_3) & 0 & L_1\cos\theta_1 + L_2\cos(\theta_1+\theta_2)+L_3\cos(\theta_1+\theta_2+\theta_3) \\ \text{sen}(\theta_1+\theta_2+\theta_3) & \cos(\theta_1+\theta_2+\theta_3) & 0 & L_1\text{sen}\theta_1 + L_2\text{sen}(\theta_1+\theta_2)+L_3\text{sen}(\theta_1+\theta_2+\theta_3) \\ 0 & 0 & 1 & 0 \\ 0 & 0 & 0 & 1 \end{bmatrix} \quad (1) $$

With,

${}^{0}T_3$ transformation matrix from RF {3} to RF {0}

L_1, L_2, L_3 link length

θ_1, θ_2, θ_3 joint angle

4.2. Model dynamics

The dynamic equations can be obtained through several methods. In this paper the Recursive Newton-Euler formulation was used to obtain the torque values at the joints.

The general equations of the movement of a manipulator of n-axes in on ground environment is given by:

$$ Q = M(q)\ddot{q} + C(q,\dot{q})\dot{q} + V(\dot{q}) + G(q) \quad (2) $$

where

q(t) vector of generalized position coordinates
Q(t) vector of generalized forces associated to q(t)
M(q) inertia tensor
$C(q,\dot{q})$ matrix of Coriolis and centripetal effects
$V(\dot{q})$ matrix of viscous and Coulomb effects
G(q) vector of gravity effects

Introducing the term $F(q,\dot{q})$ to represent buoyancy and drag forces in equation (2), gives to the following equation:

$$Q = M(q)\ddot{q} + C(q,\dot{q})\dot{q} + V(\dot{q}) + F(q,\dot{q}) + G(q) \tag{2}$$

The term $F(q,\dot{q})$ can be combined with the terms $C(q,\dot{q})$, $V(\dot{q})$ or $G(q)$. This will not be considered to evidence the different nature of the forces. The term $F(q,\dot{q})$ can be divided in other two terms: the static effects $F_S(q)$, and the dynamic effects $F_D(q,\dot{q})$.

$$F(q,\dot{q}) = F_S(q) + F_D(q,\dot{q}) \tag{3}$$

The static term depends on the generalized position coordinate, and the dynamic term also depends on the first and second derivatives of the position. The static term refers to the buoyancy force and the dynamic term refers to the drag force.

In this model, the fluid used in the analysis is the seawater, considered here as an incompressible fluid. There are two types of forces that the fluid can exert in a body (Lévesque, 1994).

- Buoyancy: this force depends on the weight of the fluid moved by the submerged body in the liquid. The resulting force always acts in the vertical direction and upwards;
- Hydrodynamic drag: this force depends on the square of the relative speed of the fluid in relation to the body; on the geometry of the body, characterized by a certain coefficient and an area of the body; and of the density of the fluid.

When the arm is completely submerged and the volume of the links is completely known, the buoyancy is simply calculated by the following equation:

$$\mathbf{F_A} = \gamma V \mathbf{z_0} \tag{4}$$

where
$\mathbf{F_A}$ buoyancy force
γ water specific weight
V link volume
$\mathbf{z_0}$ unit vector pointing upwards

The force resulting from the fluid action on the body is caused by the friction and distribution of fluid pressure around the submerged body. The vector that represents the drag forces is in the opposite direction of the body movement. The resultant force is given by:

$$\mathbf{F} = \frac{1}{2}\rho C S \mathbf{U}^2 \tag{5}$$

where
F total drag force
ρ water specific mass
C drag coefficient
S reference area
U relative velocity between the body and the fluid

$$C = C_{D,basic}\left(\sin^2\alpha_d\right) \tag{6}$$

where
$C_{D,basic}$ is the drag coefficient: dependent of the link geometry
α_d is the angle between the fluid mass and the link axis

Assuming that the link surface is a cylinder, the coefficient $C_{D,basic}$ is 1,1. This value is considered constant for the analysis. A complete overview of this topic can be found in Lévesque (1994) and Janocha (1991).

Figure (7) and Eq. (7) show the vector composition of the relative velocity **U**.

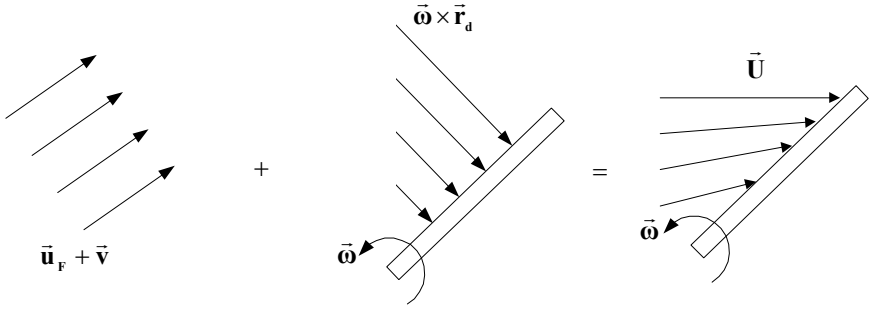

Figure 7. Link Velocity vectors.

$$\mathbf{U} = \mathbf{u}_F - \left[\mathbf{v} + (\boldsymbol{\omega} \times \mathbf{r}_d)\right] \tag{7}$$

where

U is the linear vector of relative velocity

$\mathbf{u}_F$ is the linear velocity vector of the fluid

ω is the angular velocity vector of the link

v is the linear velocity vector of the link in relative to RF origin

$\mathbf{r}_d$ is the position vector of the point along the link axis

To obtain the total drag force (Eq. 8) is necessary to perform the integration along a reference area $dS = b\, dr_d$. Here, b is the width of the rectangle that circumscribes the projection of the frontal area of the infinitesimal element and dr_d is the length of this element.

$$\mathbf{F} = \int_0^L 1/2\, \rho\, C\, U^2\, b\, \mathbf{c}\, dr_d \tag{8}$$

where

L is the link length

c is the unit vector in the force direction

And the moment around the center of mass of the link is giving by:

$$\mathbf{N} = \int_0^L 1/2\, \rho\, C\, U^2\, b\, (\mathbf{r} \times \mathbf{c})\, dr_d \tag{9}$$

where

r is the position vector of the element dr_d in relation to the link center of mass

5. Tests Facilities Scenario

A three degree-of-freedom, 1:10 scale, simplified model in aluminum of the SPA was constructed, so that the behavior of the SPA could be investigated on site. Tests were performed only in ground conditions, with the facilities installed at the Hospital of Traumato-Orthopedics (HTO), located in Rio de Janeiro.

The existing facilities is based in a commercial data acquisition product, the VICON® system. This is composed by: three cameras for video capture, a PC type microcomputer, a driver module, dedicated software and many self-adhesive reflexive marks. The equipments are mounted in a room of about 40 square meters, in a clean and airy atmosphere.

The digital files generated by the system were used for the mathematical calculation and computer simulation. The main characteristics and variables of the VICON® system are summarized below:

- The cameras will track each mark located at the joints, and each mark will be labeled as a certain point Pi;
- The output file will contain the x, y and z coordinates of each point, at a time base, related to the inertial RF of the laboratory;
- The resolution of VICON® system is ±0,5 mm.

The cameras arrangement at the laboratory can be viewed in Fig. (8) and the model in Fig. (9). The tests were executed in ground conditions, because the VICON system doesn't work when the manipulator is submerged. A comparison between the air and the fluid environment was only possible by the means of computer simulation.

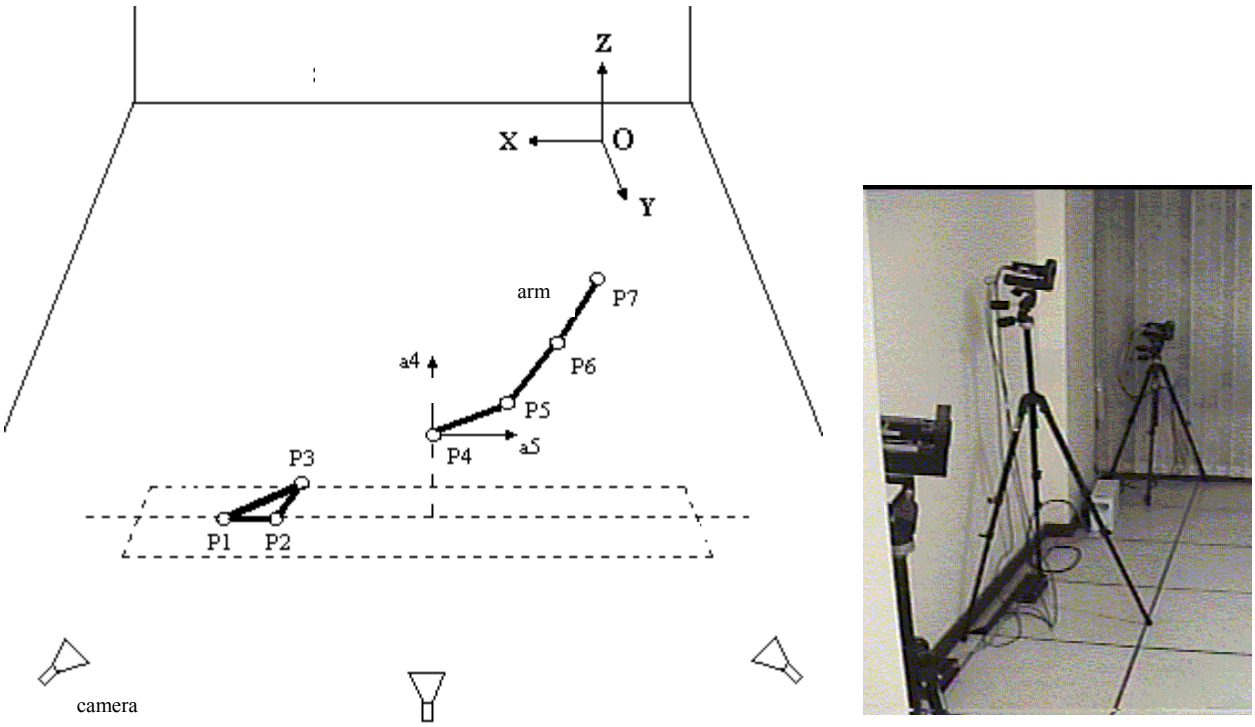

(a) (b)

Figure 8(a). Arrangements of test facilities at the laboratory. (b). Photo of the cameras on site.

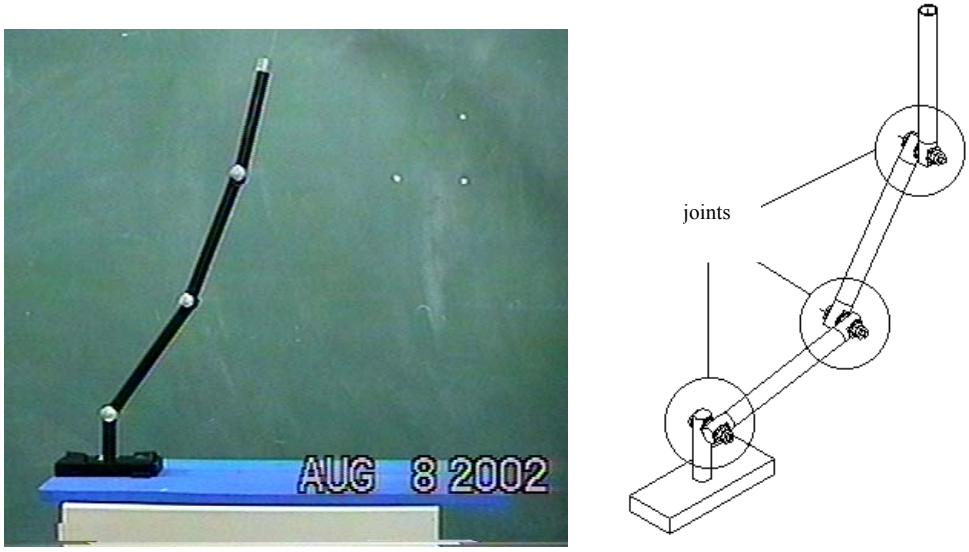

(a) (b)

Figure 9(a). Arm Photo. (b). Details of the joints.

Tests procedure can be summarized as follows:

- calibration of the simulation system;
- mounting of the arm and its leveling;
- adjustment of the lock/ unlock state of the joints;
- visualization of the marks on the screen of the monitor, and calibration of its parameters and variables;
- launching of the arm (gravity acceleration);
- capture and recording of the kinematics data with the cameras;
- repetition of the launching for the given configuration or change of configuration;
- the procedure is restarted from the beginning.

The use of the VICON system demands the execution of several algebraic procedures to obtain the widespread coordinates of the movement, for each instant of time. The system captures the Cartesian coordinates of the several points Pi, inserted in the system. These points are known as: P1, P2, P3 (reference marks located at the same plane of plane of the arm), P4, P5, P6 and P7 (arm joints itself); that correspond to the geometric places of the reflexive marks, as presented in Fig. (8a).

For each point Pi captured by the system, it can be considered the existence of a polynomial p(t) able to interpolate, with a certain error, the pairs of points (coordinate x time) along the path. The degree of the polynomial will depend on the initial and final conditions of the position, speed and acceleration that is desired to specify in the model kinematics.

The tests performed in all combinations mentioned in Table (2) show that a polynomial with degree 5 is well fitted to represent the joint position coordinate, Eq. (10).

$$q(t) = At^5 + Bt^4 + Ct^3 + Dt^2 + Et + F \tag{10}$$

where
A, B, C, D, E and F are constants
t is the instant of time

VICON system recorded each joint position (mark) and this dataset was used as input to the calculations of the kinematics and dynamics functions developed in Matlab (Cabral, 2002; Corke, 1996).

6. Tests and Results

Two steps form the analysis of each configuration: the first step regards the experimental test of the arm in ground conditions. The second step regards the mathematical simulation of the submerged arm in the water.

Here only one analysis is considered. In Cabral (2002) we can find, in sequence, the graphs of the kinematics and of the dynamics for all the twenty-one files generated by the tests in laboratory.

6.1. First step: on ground

In this first simulation, the three joints J1, J2 and J3 are free and the arm was launched starting from the point P. In Fig. (10a) it is possible to verify the path of the point P, as well as the trajectory of the three joints.

The time interval selected for the analysis ranges from 0,066s (start of the video capture) to 0,317s (the instant in which the joint J2 reaches the wooden base).

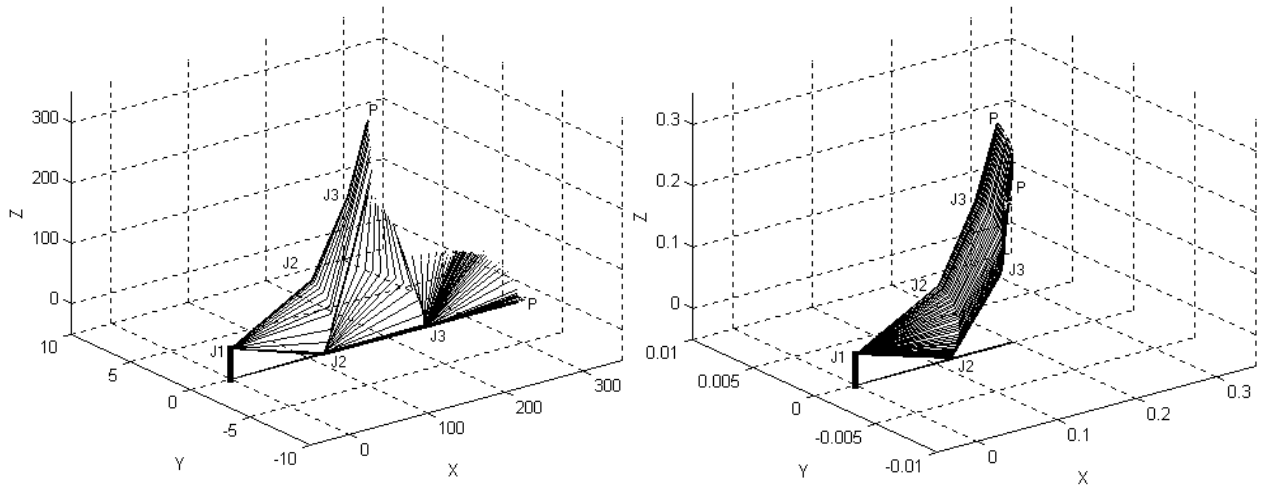

(a) (b)

Figure 10. 3D trajectories. (a) First step. (b). Second step.

For each joint angle, it is possible to express a function q(t), as presented as follows.
For the joint J1:

$$q(t) = 9437{,}6t^5 - 7330{,}9t^4 + 2126{,}4t^3 - 313{,}2t^2 + 22{,}6t \tag{12}$$

For the joint J2:

$$q(t) = -4269{,}3t^5 + 2215{,}1t^4 - 333{,}5t^3 + 36{,}6t^2 - 3{,}2t + 0{,}7 \tag{13}$$

For the joint J3:

$$q(t) = -7127{,}9t^5 + 7440{,}4t^4 - 2764{,}2t^3 + 458{,}7t^2 - 34{,}5t + 1{,}1 \quad (14)$$

These kinematics data obtained from tests and the constitutive information related to the properties of the material, dimensions and form of the bodies, are inserted in Eq. (2), so that torques at the joints can be calculated. In Table. (4) are presented the torques of the arm.

Table 4. First step results.

Result	Torques [Nm]		
	Joint J1	Joint J2	Joint J3
Maximum (module)	0,9778	0,1567	0,0253
Minimum (module)	0,0195	0,0034	0,0010
Average (module)	0,2165	0,0428	0,0117

6.2. Second step: submerged arm

For the computer calculation of the submerged arm in the water, it was chosen the kinematics parameters of the on ground condition.

A polynomial of five degree was used to represent the behavior of the angles. However, the arm was not launched from a point P. It will describe a polynomial path, as shown in Fig. (10b). It is important to mention that the boundary conditions (initials and final) for the speeds and accelerations of the joints were considered null.

Another important fact is that the arm's movement happens from top to bottom, and the buoyancy force always acts in the vertical direction and upwards. Besides, the drag force will be also opposite to the movement of the arm (Janocha, 1991).

The arm was induced to follow the mentioned path, on ground and in submerged conditions; therefore, it is possible to make a simple comparison of the values of the active torques in each joint. This comparison is illustrated in Fig. (11) for the joints J1 to J3. It is noticed that the values of the torques for the simulation in the water are greater than those obtained with the arm on ground. Table (5) summarizes the relevant values of the torques obtained for the joints J1 to J3.

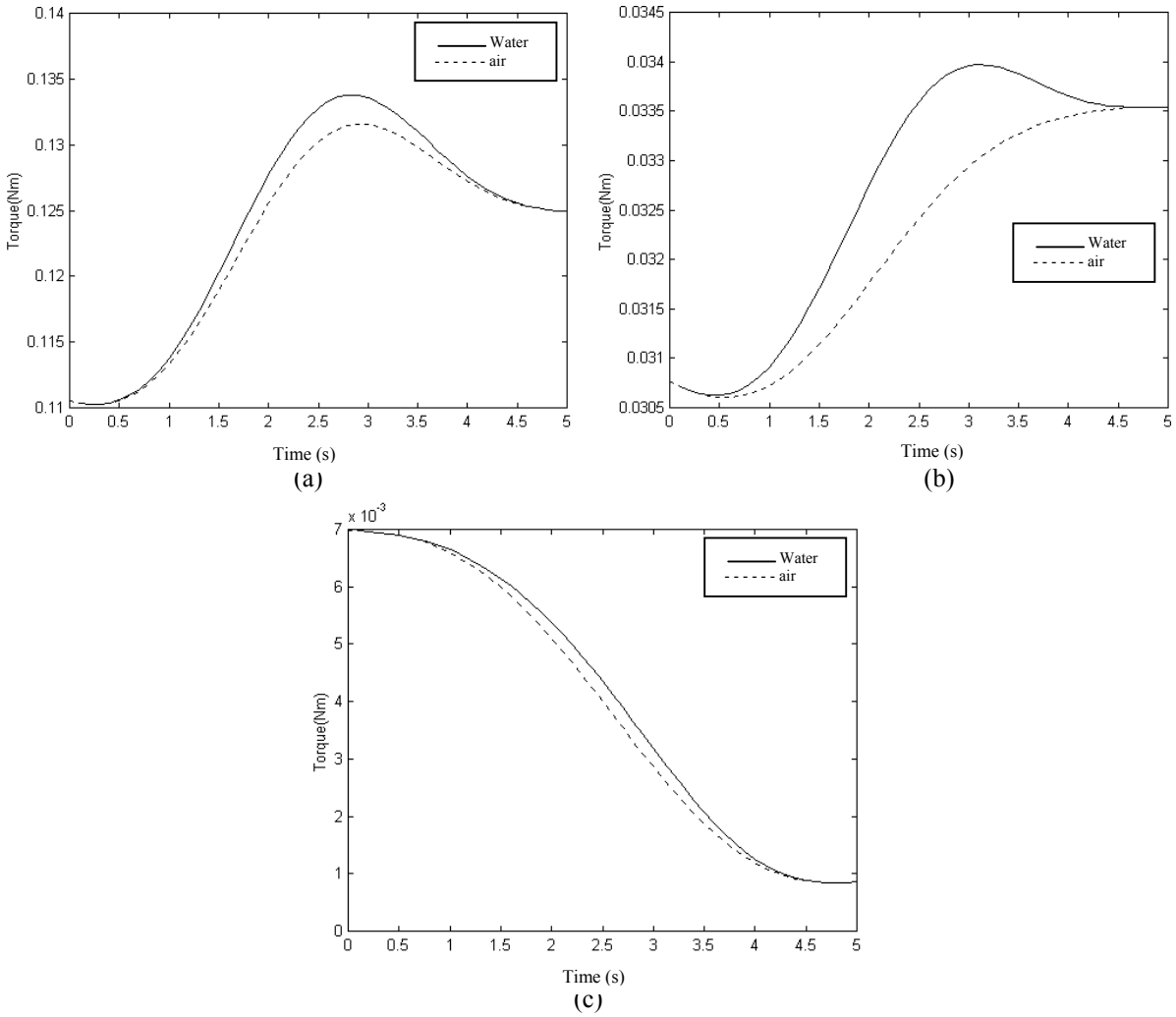

Figure 11. Torques acting at the joints: (a) Joint 1. (b) Joint 2. (c). Joint 3.

Table 5. Torques obtained in on ground and submerged conditions.

Result	Torques [Nm]					
	Joint J1		Joint J2		Joint J3	
	air	water	air	water	air	water
Maximum (module)	0,1315	0,1338	0,0335	0,0340	0,0070	0,0070
Minimum (module)	0,1103	0,1103	0,0306	0,0306	0,0008	0,0008

7. Conclusions

This article presents the new concept of a semi-passive arm (SPA) for support ROV operations and some of the fundamental principles necessary to its development. The SPA concept can be used at different configurations, according to the operational scenario and tasks to be performed.

With the kinematics data of the arm and the calculation of the mathematical dynamical model, it was possible to find the values of the existent residual torques in the joints J1, J2 and J3. The amplitude of these values is very important for the dimensioning of the brakes.

Several paths (position and time) were stored in twenty-one files and processed by functions and routines developed in MATLAB, to obtain the inverse kinematics (speed and acceleration). This whole mathematical work will be presented in future publications.

Suggestions for future works, are presented as follows:

- To improve the study of the dynamics in the fluid environment, it can be taken into account the effects of the interaction of the drainage in the adjacent area elements, as well as the interaction among the drainages in the arm links;
- Further investigations can be made regarding the shape of the arm links. This radically changes the values of the drag coefficients used in the calculation of the total drag force;
- Since the VICON system was not efficient for the tests with the submerged arm, alternative systems for capturing of the kinematics data should be considered, for instance, the use of synchronized CCD cameras;
- Other models should be investigated, taking in consideration new kinematics configurations, more degrees of freedom and effects on structural optimization, vibration and damping of the links;
- Construction of prototypes with brakes.

8. References

Andrews, J., Jacobson, J. “Deepwater Intervention: trends in remotely operated vehicles and tooling systems”. In: *III Forum sobre ROV*, pp. 10.1-10.6, Rio de Janeiro, Aug. 1993.

Assayag, M., *PROCAP 2000- Programa de Inovação Tecnológica da Petrobrás*, Petrobrás, Corporate Communication Internation Relations Office, 1998.

Cabral Junior, V.P., *Estudo da Dinâmica de um Manipulador Passivo para Suporte às Atividades de ROV's*. Tese de M.Sc., COPPE/UFRJ, Rio de Janeiro, RJ, Brasil, 2002.

Corke, P.I., “A Robotics Toolbox for MATLAB. (Release 6)”, *IEEE Robotics and Automation Magazine*, v. 3, n. 1, pp. 24-32, 1996.

Craig, J.J., *Introduction to Robotics Mechanics and Control*. 1 ed. Califórnia, Addison-Wesley Publishing Company, 1986.

Cunha, J.P.V. et. al., “Short Range Position Measurement Systems for Underwater Vehicle Dynamic Positioning”, *IEEE*, pp. 484-489, 1993.

Hsu, L. et al., “ Dynamic Positioning of Remotely Operated Underwater Vehicles”, IEEE Robotics and Automation Magazine, pp. 21 – 31, 2000, USA;

Janocha, H., Papadimitriou, I., “Simulation on the Dynamic Behavior of Robots in an Extreme Environment”, *Robotics & Computer-Integrated Manufactoring*, v. 8, n. 3, pp. 163-169, 1991.

King, D.A. “Basic Hydrodynamics”. In: Myers, J.J., Holm, C.H. (eds), *Handbook of Ocean and Underwater Engineering*, 1 ed., section 2, USA, Mc-Graw Hill, 1969.

Lévesque, B., Richard, M.J., “Dynamic Analysis of a Manipulator in a Fluid Environment”, *The International Journal of Robotics Research*, v. 13, n. 3, pp. 221-231, 1994.

Ricci, F., Ellingsen, P.B. “The REMO Project”, In: *Proceedings of ROV'92*, San Diego, 1992.

Rivin, E.I., *Mechanical Design of Robots*. 1 ed. New York, McGraw-Hill, 1988.

Sciavicco, L., Siciliano, B., “ Robotica Industriale – Modellistica e Controllo di Manipulatori”, McGraw-Hill, Italy, 374 pp., 1995.

Seaeye Marine Limited, www.seayee.com, 2003.

Romano, V.F., Scieszko, J.L., “Mechanical Aspects of a Passive Arm for ROV Dynamic Positioning Control”, Proceedings of DINAME 97 Conference on Dynamic Problems in Mechanics, pp. 122-124, Brazil, 1997.